Journal of Computational Physics 230 (2011) 6367–6378

Contents lists available at ScienceDirect

Journal of Computational Physics

journal homepage: www.elsevier.com/locate/jcp

Rotational invariance in the three-dimensional lattice Boltzmann method is dependent on the choice of lattice

Alexander Thomas White, Chuh Khiun Chong *

Department of Materials Science and Engineering, The Kroto Research Institute, North Campus, University of Sheffield, Broad Lane, Sheffield S3 7HQ, United Kingdom

ARTICLE INFO

Article history:
Received 14 December 2010
Received in revised form 24 March 2011
Accepted 23 April 2011
Available online 30 April 2011

Keywords:
Lattice Boltzmann
Isotropy
Rotational invariance
Computational fluid dynamics (CFD)
Three-dimensional

ABSTRACT

The lattice Boltzmann method has recently gained popularity as a tool for simulating complex fluid flows. It uses discrete sets of velocity vectors, or lattices, to create a reduced model of the molecular dynamics of a continuum fluid. While several lattices are believed to behave isotropically, there are reports of qualitatively incorrect results. However, thus far, the reason as to why a lack of isotropy occurs is not known. Based on the hypothesis that lower order lattices may not display rotational invariance, this study tests the isotropy of the D3Q15, D3Q19 and D3Q27 lattices by performing simulations at intermediate Reynolds numbers (50–500) and low Knudsen number (<0.0005) in an axisymmetrical geometry with a nozzle leading to a throat followed by a sudden expansion. The symmetry properties of the results were examined. It was found that at $Re \geqslant 250$ the D3Q15 and D3Q19 lattices produced different results depending on the plane of the lattice with which the flow was aligned. Lattice planes with fewer than six velocity vectors consistently produced results which were qualitatively different from the planes with six or more velocity vectors. These errors were not observed at $Re = 50$ or when a D3Q27 lattice was used. They appeared to be independent of grid density, collision operator and Ma. This suggests that the lattices which contain these planes are not fully isotropic and therefore do not properly replicate the behavior of a real fluid in this particular situation, notably downstream from the expansion. Predictions made using these models in more complex geometries may therefore be affected by the orientation of the lattice. When using LBM in CFD simulation (including validation) this study highlights the need for caution to ensure that the solution obtained is independent of the lattice orientation throughout the domain.

1. Introduction

The lattice Boltzmann method (LBM) is a procedure for performing computational fluid dynamics (CFD) simulations reported to be suitable for very complex flows, e.g. biological flows [14,26,29], flows in porous media [10] and flows incorporating complex physical phenomena such as Magnetohydrodynamics [6]. It is based on molecular dynamics as described by the Boltzmann equation with the phase space discretized from a continuum to a lattice.

The discretization of the velocity space determines what connections between lattice nodes are present and this can significantly affect the simulations. It is desirable to use the minimum number of discrete velocities which will faithfully reproduce the required macroscopic physics as this will make the most efficient use of available computational resources. For the remainder of this paper the particular discretization of the velocity space is described as the lattice and the D*n*Q*m* convention

* Corresponding author.
E-mail addresses: mtp09atw@shef.ac.uk (A.T. White), c.k.chong@shef.ac.uk, c.k.chong@sheffield.ac.uk (C.K. Chong).

0021-9991/$ - see front matter © 2011 Elsevier Inc. All rights reserved.
doi:10.1016/j.jcp.2011.04.031

for describing lattices is used. In this convention n indicates the number of dimensions and m the number of discrete velocities.

Wolfram showed that for a cellular automation fluid all moments up to (and potentially above) fourth order are complete and isotropic for a D3Q27 lattice [31]. However, lattices pruned from D3Q27 have been shown not to contain complete tensors up to such high order [28]. At least six independent variables are required by the two-dimensional (2D), athermal Navier–Stokes (NS) equations. It could be observed that the planes with the Miller index {110} on the D3Q19 lattice, as described in Fig. 1 and Table 1, have only 5 discrete velocities including the rest particles. Therefore it is hypothesized that the three-dimensional (3D) lattices which have planes with only five independent velocity vectors may not be able to properly simulate fluid behavior if the planes with nine velocity vectors, which are at 45 degrees to the planes with five velocity vectors, do not contribute sufficiently to the solution on these planes. While errors caused by the discretization of time, space and velocity would disappear in the limit of infinite resolution and converge to zero at a second order rate [19,21], errors due to a lack of isotropy may not [33].

To the authors' knowledge there have been few practical tests of the rotational invariance of the most commonly used lattices, and furthermore these tests have been performed either at high Knudsen number (Kn) [33] or low Reynolds number (Re) [18]. When Kn is low, as is usually the case for macro-scale flows of fluids with a reasonably high molecular density, lattices with relatively few velocity vectors such as D3Q13 have been observed to display physically realistic behavior [7]. However at high Kn conventional lattices have been reported to show a severe lack of rotational invariance in a 2D study [33]. At low Kn many studies have been performed using one or two of the lattices employed in this study over a range of Re without a lack of rotational invariance being reported, e.g. [14,18,20]. However, Harrison did report velocity profiles which were not axisymmetrical in an axisymmetrically constricted tube [13], and Mayer and Házi reported qualitatively incorrect results for D3Q19 but not D3Q27 [23]. The reason for the errors observed by Harrison and Mayer and Házi has not been investigated to date. This study tests the rotational invariance at moderate Re between 50 and 500 and Kn below 0.0005 of the D3Q15, D3Q19 and D3Q27 lattices by performing simulations in an axisymmetrical geometry which would be expected to produce axisymmetrical results if a lattice was fully isotropic. The effects of grid density and Mach number (Ma) were tested to determine if any errors observed would disappear in the limit of infinite resolution. Simulations were also performed using different collision operators to test whether the isotropy of the results is influenced by the choice of collision operator.

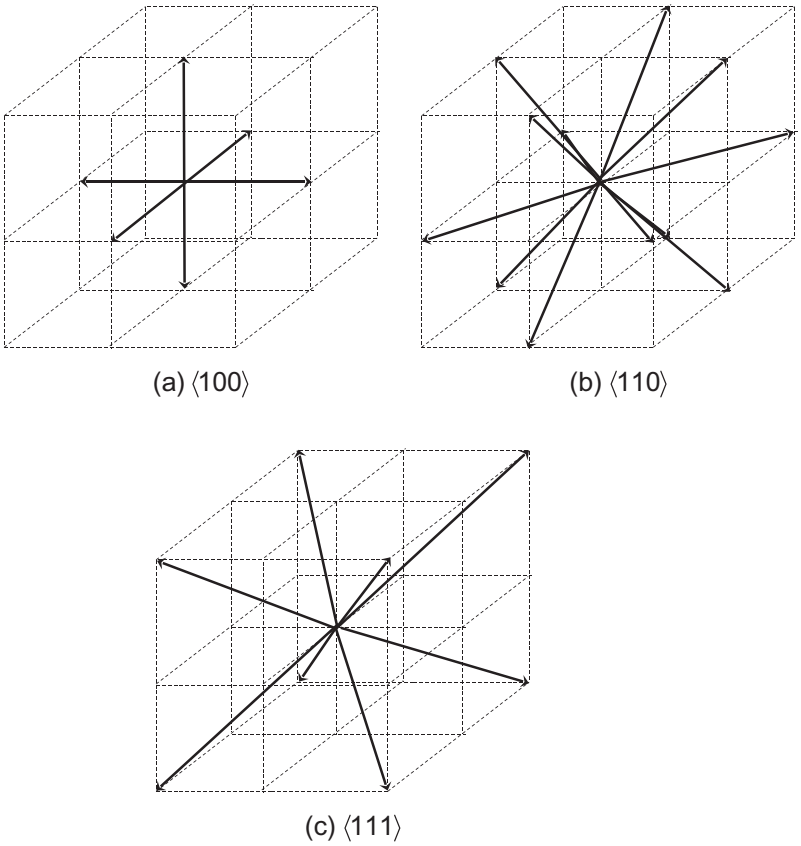

Fig. 1. Sets of velocity vectors described by different Miller indices.

Table 1
Weights of velocity vectors present on different lattices.

Miller index	Length	D3Q15	D3Q19	D3Q27
[000]	0	2/9	1/3	8/27
⟨100⟩	1	1/9	1/18	2/27
⟨110⟩	$\sqrt{2}$	0	1/36	1/54
⟨111⟩	$\sqrt{3}$	1/72	0	1/216

Many studies have validated LB models against analytical solutions of the NS equations, e.g. [1,3]. These validations can give precise values for the errors produced by each model, as the required solution is known exactly for the entire domain. The complexity of the flow must necessarily, however, be relatively low in order for an analytical solution to the NS equations to be obtainable. Furthermore, models validated using simple flows may not be applicable to more complex flows. Therefore in this study we use a complex flow condition which is challenging to model but for which quantitative measures of error are not possible.

2. Methods

2.1. The lattice Boltzmann method

LBM was originally proposed as an improvement to lattice gas cellular automata (LGCA) [17,24]. However it has been shown that the NS equations can be derived directly from the LB equation (LBE) [27] and the LBE can be obtained directly from the Boltzmann equation [16].

The LBE is frequently expressed in the following form:

$$f_i(x+\mathbf{e}_i dt, t+dt)dxdp - f_i(x,t)dxdp = \frac{\partial f_i(x,t)}{\partial t}_{collision} dxd\rho dt \tag{1}$$

where the terms on the left represent the free streaming of the particles and the term on the right accounts for intermolecular collisions. A collision operator which has become popular due to its simplicity and efficiency is the Bhatnager, Gross, Krook (BGK) collision operator [2,4]. At each time step this operator simply relaxes all of the particle populations at a uniform rate towards a local equilibrium distribution function found from the local density and velocity by the equation:

$$f_i^{eq} = \rho\omega_i\left(1+\frac{\mathbf{e}_i\cdot\mathbf{u}}{c_s^2}+\frac{(\mathbf{e}_i\cdot\mathbf{u})^2}{2c_s^4}+\frac{\mathbf{u}\cdot\mathbf{u}}{2c_s^2}\right) \tag{2}$$

where the vectors $\mathbf{e}_i$ and $\mathbf{u}$ represent respectively the velocity components in each direction and the local velocity vector. c_s represents the speed of sound in lattice units and is typically $1/\sqrt{3}$. BGK can therefore be regarded as a single relaxation time collision operator. Variations on this collision operator which simulate fully incompressible flows [15] or improve the numerical stability compared to the standard BGK model [22] have been reported. Multiple relaxation time (MRT) models have also been reported to significantly improve numerical stability and potentially greatly reduce computational effort by allowing simulations to be performed on much smaller grids [8].

2.2. Lattices

Each of the three lattices, D3Q15, D3Q19 and D3Q27, is based on a cube and can be formed by a combination of the sets of Miller indices shown in Fig. 1. The lattices can also be described mathematically by the sets of Miller indices with the respective lengths and weights, as shown in Table 1. The lattices are only invariant with certain rotations about their axis. However, to properly model a continuum fluid their properties must not change with any arbitrary rotation. Therefore the tensors derived from moments of the distribution function which give the values of the macroscopic variables density, ρ, velocity $\mathbf{u}$ and momentum flux $\mathbf{\Pi}$ as shown by Eqs. (3) and (5) must be fully isotropic.

$$\mathbf{M}_1 = \rho = \sum_{i=1}^{n} f_i \tag{3}$$

$$\mathbf{M}_2 = \mathbf{u} = \sum_{i=1}^{n} f_i e_i \tag{4}$$

$$\mathbf{M}_3 = \mathbf{\Pi} = \sum_{i=1}^{n} f_i e_i e_i \tag{5}$$

2.3. Simulation setup

The LBM simulations in this study employ the open source software library Palabos (http://www.lbmethod.org/palabos). Palabos is written in C++ and implements various LB models. It is capable of running either in serial or in parallel. The 3D geometries were read from stl files created using SoildWorks (SolidWorks Corp. Concord, MA, USA). A voxelization process was then implemented using the open source C++ library CVMLCPP (http://tech.unige.ch/cvmlcpp/). This produced a lattice with only fluid and solid nodes. It should be noted that no smoothing of the edges was implemented in this study. This was acceptable as a highly accurate solution near the boundaries was not necessary to achieve the aims of this study.

The geometry studied is a nozzle design as shown in Fig. 2. This geometry was chosen for this study for a number of reasons. Firstly, it is simple and axisymmetrical but challenging to model due to the sudden expansion. Secondly, and more importantly, it is a benchmark flow model employed in the US Food and Drug Administration (FDA) Critical Path Initiative Project [12] to determine the applicability and limits of current CFD simulations in evaluating medical devices, i.e. to better study the interaction of flowing fluids with medical devices, an area in which the application of LBM has already been reported [26,29] and which is expected to become increasingly popular and important. Therefore it is appropriate that LBM is tested using this benchmark flow model. The diameter ratio between the throat and the expansion is 1:3, causing an approximately nine fold increase in velocity from the inlet to the end of the throat. Studies were performed at *Re* of 50, 250 or 500 based on the average velocity and diameter at the throat. The effect of increasing *Re* was to make the flow more complex and therefore more challenging to model. *Kn* was calculated using the following equation [30]:

$$Kn = \frac{l_m}{H} = \frac{v}{c_s H} \tag{6}$$

where l_m is the molecular mean free path, H is the shortest length scale, taken in this case to be the diameter of the throat in lattice units, v is the kinematic viscosity and c_s is the speed of sound. *Kn* was below 0.0005 in all simulations.

Simulations were performed either in serial or parallel on the Iceberg supercomputer at the University of Sheffield on 64 bit AMD processor cores. In all simulations a Dirichlet boundary for velocity was imposed at the inlet applying a constant fully developed parabolic velocity profile. At the outlet a zero gradient condition was applied on all particle populations. All solid nodes applied a bounce back boundary condition.

The simulations comparing the effect of grid density and those at $Re \leqslant 250$ used the BGK collision operator as it has been shown to be extremely efficient [4]. The results comparing different lattices at *Re* = 500 were obtained using the regularized BGK collision operator as it improves numerical stability with a minimal effect on computation time [22]. The final results with either collision operator when other variables were kept constant were observed to be in close agreement as discussed in Section 3.1.

While LBM has been shown to be second order accurate for velocity and shear stress fields [21], it is accepted that in this 3D study on a complex domain at fairly high *Re* the computational cost of performing calculations on a grid with sufficient cells to achieve second order accuracy is prohibitive. Therefore it is sufficient to ensure that changes introduced by increasing the grid density are as small as possible. The diameter of the section was represented by at least 60 lattice nodes for all simulations at *Re* = 500. However, due to the reduced complexity expected at lower *Re* the diameter was represented by at least 52 lattice nodes for the simulations at $Re \leqslant 250$. A mesh independence test at *Re* = 500 using the D3Q19 lattice and BGK

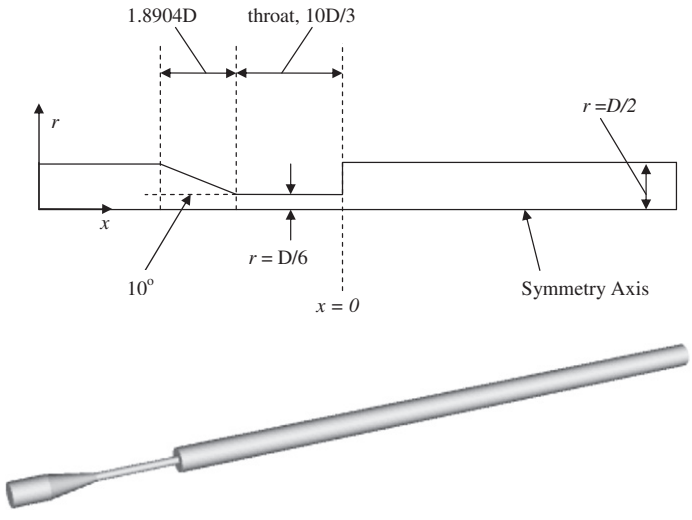

Fig. 2. Geometry in which simulations are performed (Not to scale). The outlet is kept sufficiently long so that when the flow leaves the domain it is fully developed. The location at the expansion ($x = 0$) is used as reference point for the discussion of results.

collision operator showed that at this density a change in cell number of 20% resulted in a value of ϵ, as defined by Eq. 7 (taking u_1 and u_2 to be the centreline velocity profiles for the two simulations), of less than 5%. The overall flow structure was very similar between the two cases and the change in the maximum observed velocity was less than 2%, as shown in Table 2. All simulations were run until converged. For the simulations at Re = 50 and 250 at least 120,000 iterations were performed while for Re = 500 at least 150,000 iterations were required for convergance. Expressed in non dimensional convective units defined as $t_d = l_{0,lB}/u_{in,lB}$, where t_d is the non dimensional time unit, $l_{0,lB}$ is the maximum diameter of the tube in lattice units and $u_{in,lB}$ is the average applied inlet velocity, the minimum simulation times were 16.4 for Re = 500, 12 for Re = 250 and 3 for Re = 50.

2.4. Quantification of Asymmetry

The asymmetry of the results was quantified by examining the disagreement between the axial velocity profiles along different lines which passed through the central axis of the flow at the same location:

$$\epsilon = 100 \times \frac{\sum_{i=0}^{D} |u_1 - u_2|}{0.5 \sum_{i=0}^{D} (u_1 + u_2)} \tag{7}$$

where ϵ is a measure of the asymmetry and u_1 and u_2 are the velocity profiles along two lines at equivalent axial positions but rotated through 45°. As lattice nodes were not at the same locations along the two lines, linear interpolation and extrapolation was performed to obtain u_2 with nodes located at the same distance from the centreline as u_1. When performing the extrapolation values of zero were imposed on soild nodes. Clearly for an axisymmetrical flow ϵ will be equal to zero.

3. Results

Rotational invariance was tested by examining velocity contour plots on cross sections at various locations upstream ($x > 0$) or downstream ($x < 0$) from the expansion and by comparing the velocity profile along lines passing through the central axis of the section. The lines which were examined passed through the flow axis and were parallel to either the [010] or [011] vector, assuming that the [100] vector is parallel to the central axis of the geometry. The velocity plots on lines which were equivalent but rotated through 90 degrees about the centreline were found to be in close agreement in all simulations provided sufficient iterations were performed. Fig. 3 shows the velocity contour plots at Re = 500 at $x = +4D$ taken from D3Q19 and D3Q27 lattices with the diameter of the section represented by 60 lattice nodes using the regularized BGK collision operator. Fig. 4 shows graphs of the velocity from the same simulations at the same location along the [010] and [011] vectors for the D3Q19 and D3Q27 lattices. Both lattices show results which agree well along the [010] vector. However, a significant deviation is present between different planes for the D3Q19 lattice, with the (011) plane which has the fewest velocities showing results which are qualitatively different from those on the (010) plane and the D3Q27 lattice. The asymmetry as quantified by Eq. 7 was 73.61% for D3Q19 and 1.20% for D3Q27.

Fig. 5 shows similar problems for the D3Q15 lattice at the lower Re of 250, with ϵ = 67.52%. For the D3Q15 lattice the results on the (010) plane are similar to those on the (011) plane of the D3Q19 lattice and *vice versa*. It is worth noting that simulations with Re = 500 could not be obtained on the D3Q15 lattice due to numerical instability. It has previously been observed that the D3Q15 lattice is less stable than D3Q19 [25].

3.1. Effect of collision operator

Simulations were also performed using a standard BGK, regularized BGK and MRT collision operators on a D3Q19 lattice at Re = 500. As shown in Fig. 6 these collision operators did not improve the axisymmetry, with values of ϵ of 72.98% for MRT, 72.71% for BGK and 72.48% for the regularized BGK simulation.

3.2. Effect of Reynolds number

To investigate the effect of flow complexity, simulations were performed in the same geometry on a D3Q19 lattice but at lower Re. Fig. 7 shows the difference between axial velocity plots taken at $x = +4D$ on either the (010) or (011) plane for

Table 2
Values of ϵ for different grid densities at $x = +4D$.

Diameter (lattice units)	Ma	ϵ	u_{max}
48	0.0779	66.38%	8.56
54	0.0545	71.04%	8.29
60	0.0545	73.21%	8.16
64	0.0545	71.29%	8.22
64	0.0468	72.50%	8.23

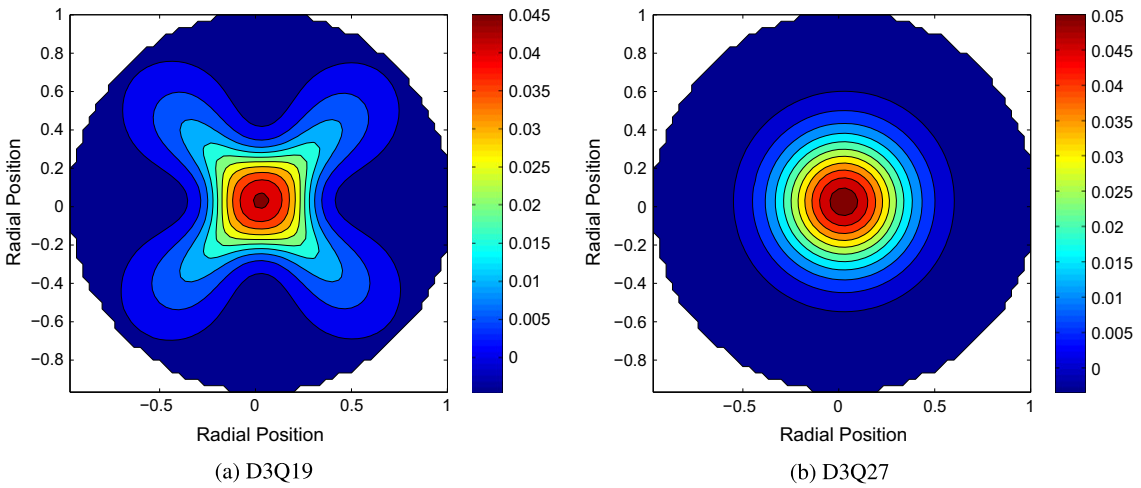

Fig. 3. Contours of axial velocity from different lattices, $x = +4D$, $Re = 500$, $Ma = 0.0545$, regularized BGK collision operator.

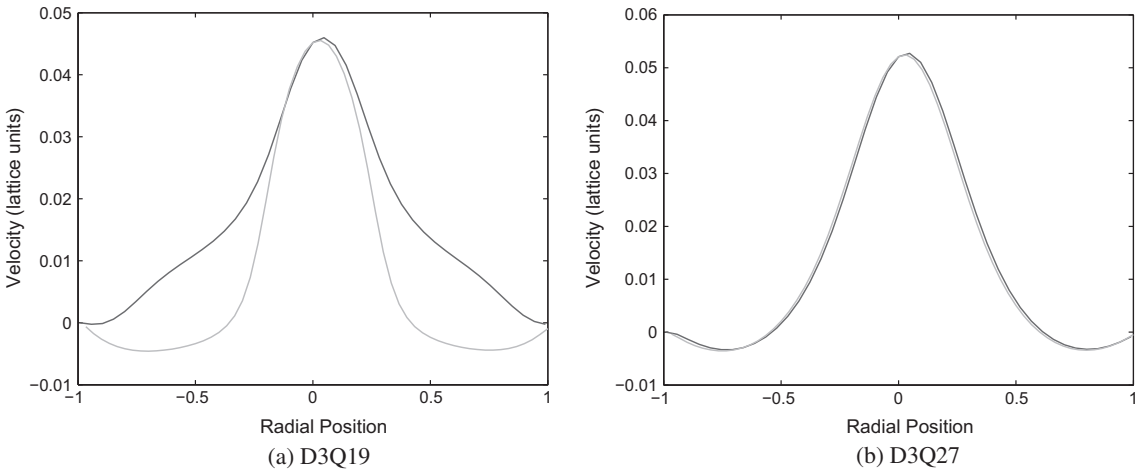

Fig. 4. Graphs of axial velocity on the (010) plane (light grey) and the (011) plane (dark grey) from different lattices, $x = +4D$, $Re = 500$, $Ma = 0.0545$, regularized BGK collision operator.

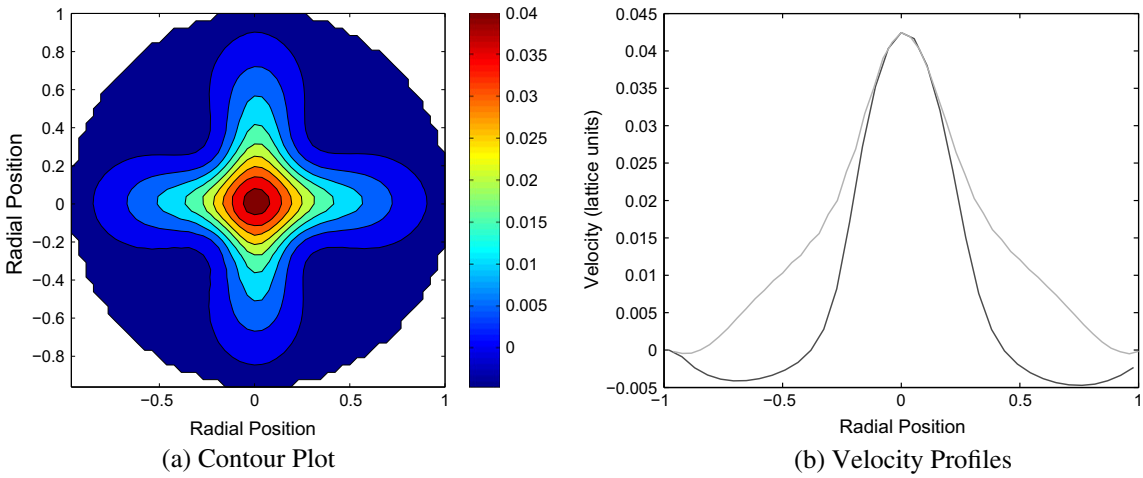

Fig. 5. Contour plot and graph of axial velocity on the (010) plane (light grey) and the (011) plane (dark grey) on D3Q15 lattice, $x = +2D$, $Re = 250$, $Ma = 0.0468$, BGK collision operator.

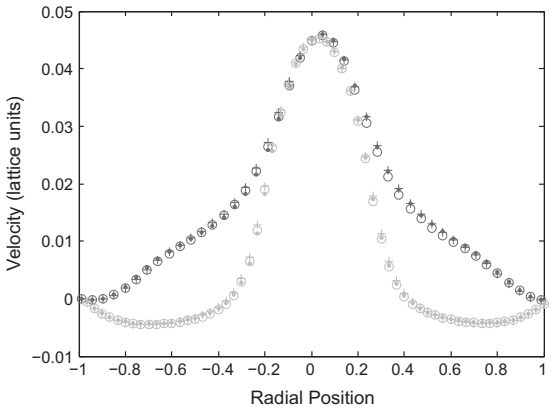

Fig. 6. Graphs of axial velocity on the (010) plane (light grey) and the (011) planes (dark grey) for standard BGK (○), regularized BGK (solid dots) and MRT (+) collision operators on D3Q19 lattice, $Re = 500$, $Ma = 0.0545$, $x = +4D$.

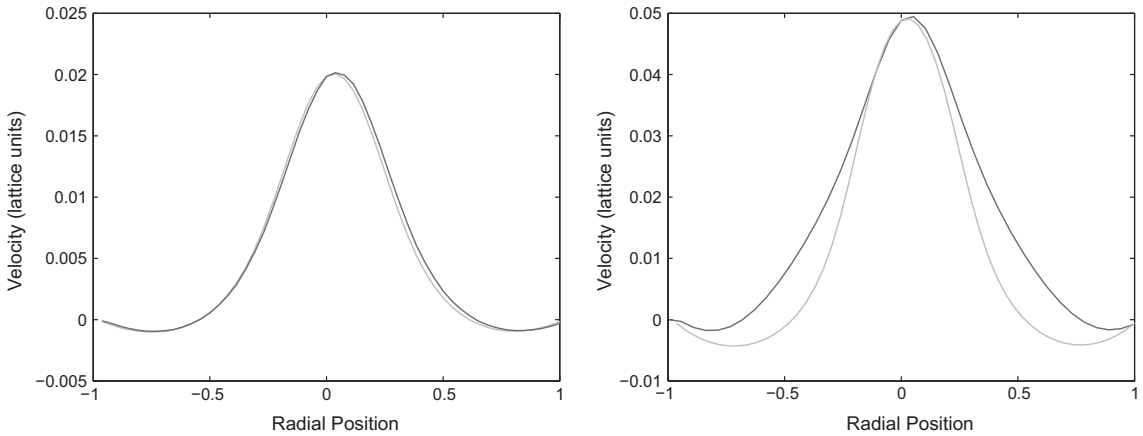

(a) $Re = 50$, $x = +0.5D$, $Ma = 0.0218$ (b) $Re = 250$, $x = +2D$, $Ma = 0.0545$

Fig. 7. Graphs of axial velocity at different Re on (010) plane (light grey) and (011) plane (dark grey), BGK collision operator on D3Q19 lattice, $Ma = 0.0545$.

simulations at $Re = 50$ and $Re = 250$. It is evident that only the simulation at $Re = 50$ shows rotational invariance. The simulations at $Re = 250$ show different solutions on different planes, with $\epsilon = 38.39\%$. Similar features are observed at $Re = 500$ (Fig. 4a). It should be noted that the value of ϵ produced by the D3Q19 lattice is lower than that produced by D3Q15 at the same Re (67.52%).

3.3. Effect of grid density

Table 2 shows ϵ and u_{max}, the maximum velocity observed along the centreline normalized against the maximum inlet velocity, at location $x = +4D$ for different sized grids applying a D3Q19 lattice and BGK collision operator at $Re = 500$. At very low grid density ϵ was observed to be at a minimum, after which little change was observed. It could be observed that changes in u_{max} introduced by increasing the resolution beyond 54 lattice nodes per diameter were less than 2%. This was the case both when simulations were performed at constant Ma and when Ma was decreased with increasing mesh density.

3.4. Effect of Mach number

To investigate the effect of fluid compressibility, simulations were performed at equivalent Re (500) and with equal grid spacing (60 lattice units diameter) but for different Ma, defined as

$$Ma = u_{throat}/c_s \tag{8}$$

where u_{throat} is the average velocity inside the throat and c_s is the speed of sound, equal to $1/\sqrt{3}$ in lattice units. Table 3 shows that for Ma around 0.0545 the results are not strongly affected by changes in Ma, with both doubling to 0.109 and halving to 0.0275 having effects of less than 2% on both ϵ and u_{max}.

Table 3
Values of ϵ and u_{max} for different *Ma*.

Ma	u_{max}	ϵ
0.109	8.288	73.41%
0.0545	8.170	72.48%
0.02725	8.184	73.62%

3.5. Axisymmetry at different locations

The axisymmetry of the results was also examined upstream from the expansion, both in the nozzle and the throat. It was found that the results before the expansion were fairly axisymmetrical in all 3 cases, with low values of ϵ at all locations studied. In the throat for the D3Q19 lattice the values of ϵ were around 6%. For the D3Q27 simulation the velocity inside the throat was slightly increased ($\leqslant$ 10%) compared to the D3Q19 simulation. Far downstream, at a location $x \approx +25D$ for $Re = 500$, all lattices showed axisymmetrical results and recovered a Poiseuille velocity profile. Figs. 8 and 9 show the development of the velocity profile for the D3Q19 and D3Q27 lattices at $Re = 500$ using a regularized BGK collision operator. From these two figures one can clearly observe that the velocity profile is strongly dependent on the chosen plane for the D3Q19 lattice but not for D3Q27.

4. Discussion

We have shown that the choice of lattice used in LBM simulations for viscous, athermal flows at low *Kn* can significantly affect the accuracy of the simulations due to a lack of rotational invariance on certain lattices. The lack of rotational invariance was present irrespective of grid density, suggesting an insufficiency in the lattice rather than errors due to an unresolved simulation. The lower value of ϵ at the lowest grid density was likely to be due to the increased effect of discretization errors at this low density rather than an improved simulation.

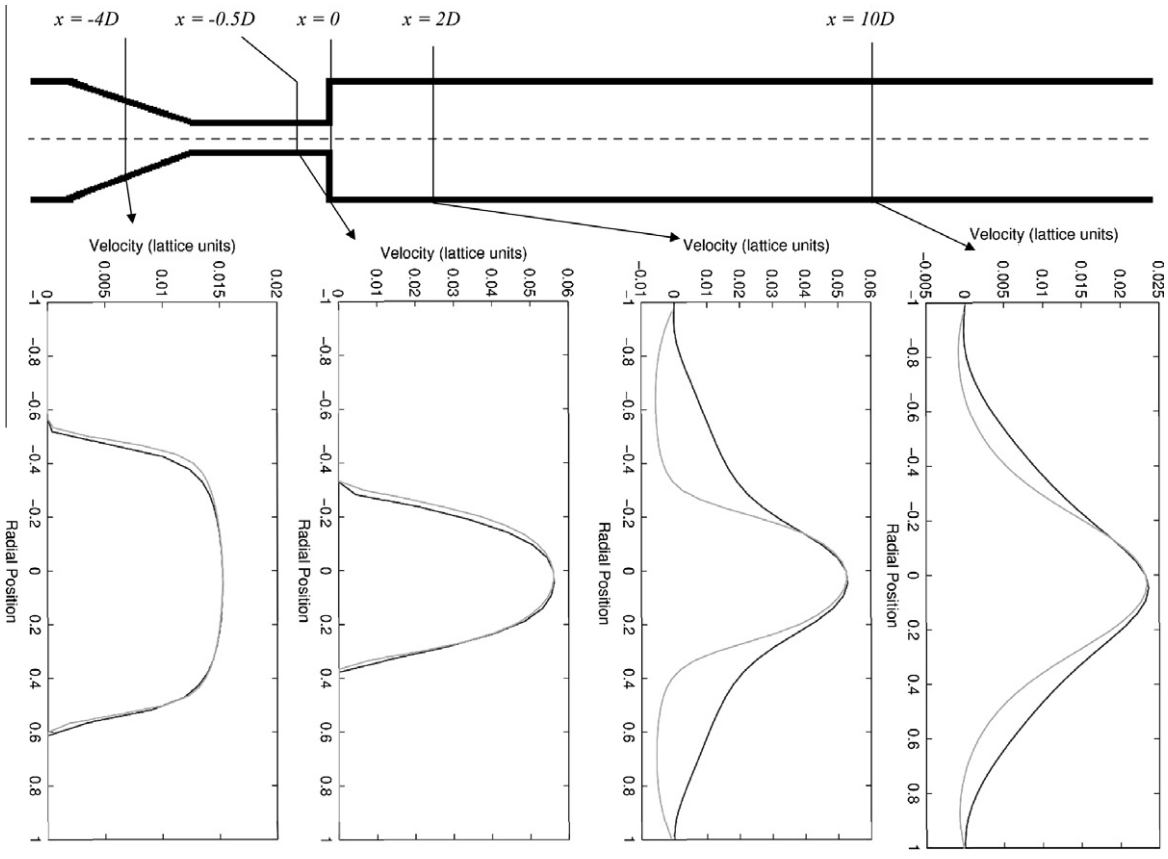

Fig. 8. Development of velocity profile on (010) plane (light grey) and (011) plane (dark grey) at different locations for D3Q19 lattice.

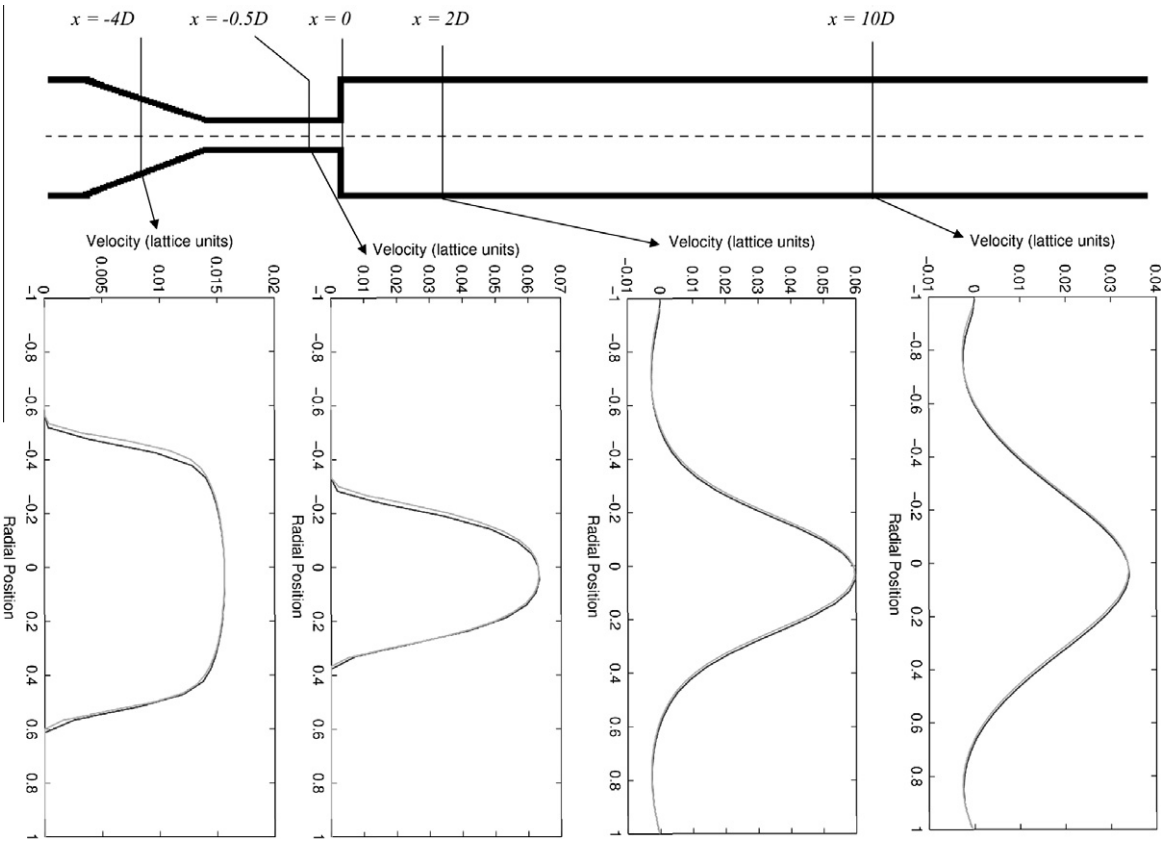

Fig. 9. Development of velocity profile on (010) plane (light grey) and (011) plane (dark grey) at different locations for D3Q27 lattice.

The lack of rotational invariance observed in this study may be due to the lack of velocity vectors in certain planes causing parts of the solution to be inadequately resolved. While this insufficiency is most obvious for axisymmetrical flows it may have a significant and undetected effect on flows in different geometries. This effect may be particularly important if LBM is being used to make predictions for real world problems for which no analytical solution, as is the case in this study, or experimental data are available for cross examination or validation. Clearly, however, the main benefit of all CFD, including LBM could only be realized if it is able to accurately model flows in such situations, including the testing and design of medical devices.

The (011) plane on the D3Q15 lattice was the plane with the fewest velocity vectors which showed qualitative agreement with the results on the D3Q27 lattice. The planes which did not agree were the (010) plane on the D3Q15 lattice and the (011) plane on the D3Q19 lattice, both of which have only five velocity vectors. This may be significant because the athermal, 2D NS equations require six independent components (pressure/density, two components of velocity and three components of the symmetrical mass flux tensor) to be fully defined. An analogy could be drawn between the planes with only five velocity vectors and the Hardy–Pomeau–de Pazzis (HPP) 2D lattice with four non zero velocities employed for LGCA [11]. This lattice has been shown earlier to be unable to properly recover the NS equations [9]. It is postulated that the planes which also have only four non zero velocities may show similar problems to this lattice when complex flow features are aligned with the plane because too few velocity vectors are present.

The effect of reducing *Re* was to reduce the expected flow complexity and improve the axisymmetry of the results. This would suggest that at higher *Re* the increased flow complexity is too much for the planes with fewer velocity vectors to accurately model, causing non axisymmetrical results. It is hypothesized that the lack of rotational invariance being present only at higher *Re* is because the five velocity planes are capable of modeling fluid behavior when complexity is low, in a similar manner to the HPP model for cellular automation. However, when the fluid displays more of the richness of the NS equations these planes are unable to fully capture it. Our results support this hypothesis, as when *Re* is high all planes with only five velocities show incorrect results. Under this circumstance it would be unlikely that similar problems would be observed when 2D lattices are used, as they have only one plane, and for all commonly used lattices this plane contains sufficient velocity vectors. The D3Q15 lattice showed poorer agreement than the D3Q19 lattice when simulations were performed at equivalent *Re*. This suggests that D3Q15 is less suitable for modeling complex flows than D3Q19 and that it would begin to show a lack of rotational invariance at lower *Re* than D3Q19. On the other hand when compared to D3Q27 (Fig. 9), the

insufficiency of the D3Q19 lattice is clearly demonstrated as it shows a very clear lack of rotational invariance downstream from the expansion where the flow is complex (Fig. 8).

The non axisymmetrical velocity profiles presented here have been observed previously in similar simulations by Harrison, using a D3Q19 lattice [13], in which the velocity contour plots observed were quatitatively similar to those observed in this study. Mayer and Házi also observed qualitatively incorrect results when using a D3Q19 lattice but not when using D3Q27 [23]. While the flow condition employed by Mayer and Házi was more complex than that used in this study, the results were similar in that the velocity contours in each quadrant were in close agreement, suggesting that their results depended upon the plane of the lattice with which the flow was aligned. Our results, coupled with the problems observed by Harrison and Mayer and Házi, suggest that when performing simulations in axisymmetrical geometries incorrect results may be present on certain planes of the D3Q15 and D3Q19 lattices even when the grid density is sufficiently high. These observations also highlight the importance of checking that simulation results are independent of lattice orientation in all geometries, as the problems present in the axisymmetrical geometry studied here may have more subtle effects in more complex geometries. As these results showed localized regions in which solutions were qualitatively incorrect they also highlight the importance of checking the solutions throughout the domain when validating CFD models against experimental data or analytical solutions.

It should be acknowledged that errors due to the discretization of time and space are present in all CFD. In LBM errors are also introduced by compressibility, which are related to the discretization of time because the velocity used in a simulation (in lattice units), and therefore *Ma*, must be larger when a larger timestep is used. It is expected that these errors would only disappear in the limit of infinite resolution of time and space. It was found in this study that compressibility errors were very small with negligible change in maximum observed velocity and small changes in ϵ when *Ma* was halved or doubled from 0.0545. Therefore, to accelerate convergence all simulations at *Re* = 500 or 250 were performed with *Ma*, based on the average velocity in the throat, close to 0.05 as this made the maximum observed *Ma* close to 0.1. Errors due to the discretization of space were also small, with changes in maximum observed velocity of less than 2% at *Re* = 500 provided the diameter of the geometry was covered by at least 54 lattice nodes, which was the case in this study.

It should be noted that the relaxation parameters used in this study were fairly low at all times. This was, however, necessary because *Re* was determined by the diameter of the throat, the mean velocity inside the throat and the lattice viscosity by the formula:

$$Re = \frac{ud}{v} \tag{9}$$

Available computational resources limited the diameter of the throat to around 20 lattice units, as the overall length had to be around 100 times greater than the diameter of the throat to ensure fully developed flow at the outlet. The requirement that *Ma*, as determined by Eq. 8, should be approximately 0.05 made the maximum viscosity for the required *Re* of 500 approximately 0.0025, corresponding to a relaxation time of 0.50075 which is lower than that required for optimal numerical stability and accuracy [21]. However, it is expected that increasing the relaxation parameters to the levels suggested by Kruger et al. [21] would not change the overall result and would simply result in a very slow simulation at this relatively high *Re*. It was initially thought that the improvement in axisymmetry at lower *Re* was due to the increased lattice viscosity. However, in the simulation at *Ma* = 0.109 and *Re* = 500 shown in Table 3 the viscosity was twice that used in the simulations at *Ma* = 0.0545 and the results were not significantly affected.

It should also be noted that, in this study, the walls were approximated by steps with no boundary smoothing performed. While this may have had a fairly significant effect on the accuracy of the solution near the wall it is unlikely that the overall flow patterns were significantly affected. As the boundary shape was not particularly complex and the resolution used in all simulations was fairly high to ensure near grid independence, the geometrical error is likely to have been fairly low. However, if convergence up to second-order accuracy was required then a more accurate boundary treatment would be necessary because the convergence of the geometrical error introduced at the walls is less than second-order. The small ϵ and the slightly increased velocity inside the throat mentioned in Section 3.5 could have been due to the lack of geometrical resolution which was highest in the throat due to its small diameter. However this geometrical error is unlikely to affect the symmetry properties downstream from the throat since the diameter of the expansion is three times larger than that of the throat. If required, interpolated boundary conditions could be implemented; this is expected to significantly improve the geometrical accuracy and eliminate these errors as demonstrated by Chang et al. [3]. Harrison hypothesized that the non axisymmetrical velocity profiles may have been due to the geometrical error at the boundaries [13]. However, this is unlikely to be the case, as Mayer and Házi also observed similar problems when interpolated boundary conditions were used [23].

When performing simulations using LBM, the choice of lattice, beside the flow complexity and grid density, significantly affects both the computational expense and the accuracy. In this study the simulations using D3Q27 were more computationally expensive than those at equivalent *Re* using D3Q19 as grid size was the same. However as the accuracy was significantly better this extra cost was justified. While the results of this study showed the D3Q27 lattice performed well it is acknowledged that the results presented here are limited to the system for which they were obtained. It is possible that for other systems or for similar systems with more complex flows than those investigated here, the 4th order isotropy displayed by D3Q27 may be insufficient. If this were the case, it would then be interesting to investigate if the recently reported higher order lattices [5] or the off lattice D3Q27 model [32] which displays 6th order isotropy would be more appropriate than the D3Q27 lattice. Further tests of the standard D3Q27 lattice to show whether or not its isotropy is sufficient, in flow

systems beyond that investigated here, would therefore be beneficial, as it offers advantages such as reduced computational expense compared to the higher order model and simpler advection compared to the off lattice model. Nevertheless computational cost efficiency should not be at the expense of the accuracy of the solutions and higher order lattices should be used when increased accuracy clearly outweighs any possible loss in efficiency, as was the case in this study. It is currently not possible to determine, *a priori*, the lowest order lattice which will produce acceptable results. Therefore further work to determine the specific circumstances in which different lattices are capable of producing adequate results would be beneficial.

5. Conclusions

This study has investigated rotational invariance of the D3Q15, D3Q19 and D3Q27 lattices based on the hypothesis that lower order lattices may not display rotational invariance. It was found that the D3Q19 lattice did not produce axisymmetrical results for an axisymmetrical flow, with the solutions on the {011} planes which have only 5 independent velocities showing significantly different results to the {010} planes which have 9 velocities. These results were found using a variety of popular collision operators and were shown to be independent of grid density and *Ma*. They were present at $Re = 250$ and 500 but not at $Re = 50$. Qualitatively similar problems were present on the D3Q15 lattice with results which appeared to be incorrect on planes with the fewest velocity vectors. This suggests that the D3Q19 and D3Q15 lattices may not be capable of faithfully reproducing realistic flows which have complex flow features aligned with the planes containing only five velocity vectors. This may be due to the fact that a five velocity lattice has insufficient independent components to properly recover the 2D, athermal NS equations. Predictions made using these lattices in more complex geometries may therefore be affected by the lattice orientation. When performing such studies caution should be used to ensure that the solution obtained is independent of the lattice orientation throughout the domain.

Acknowledgements

The authors thank the developers of Palabos and CVMLCPP as their code was very useful in performing this work and Dr. Sandy Stewart of the FDA for providing the nozzle design geometry. The funding from EPSRC is also gratefully acknowledged.

References

[1] S. Ansumali, I.V. Karlin, H.C. Öttinger, Minimal entropic kinetic models for hydrodynamics, Europhys. Lett. 63 (6) (2003) 798–804.
[2] P.L. Bhatnagar, E.P. Gross, M. Krook, A model for collision processes in gases. I. Small amplitude processes in charged and neutral one-component systems, Phys. Rev. 94 (3) (1954) 511–525.
[3] C. Chang, C.H. Liu, C.A. Lin, Boundary conditions for lattice Boltzmann simulations with complex geometry flows, Comput. Math. Appl. 58 (5) (2009) 940–949.
[4] S. Chen, G.D. Doolen, Lattice Boltzmann method for fluid flows, Annu. Rev. Fluid Mech. 30 (1) (1998) 329–364.
[5] S.S. Chikatamarla, C.E. Frouzakis, I.V. Karlin, A.G. Tomboulides, K.B. Boulouchos, Lattice Boltzmann method for direct numerical simulation of turbulent flows, J. Fluid Mech. 656 (2010) 298–308.
[6] P.J. Dellar, Lattice kinetic schemes for magnetohydrodynamics, J. Comput. Phys. 179 (2002) 95–126.
[7] D. d'Humires, M. Bouzidi, P. Lallemand, Thirteen-velocity three-dimensional lattice Boltzmann model, Phys. Rev. E 63 (2001) 066702.
[8] D. d'Humires, I. Ginzburg, M. Krafczyk, P. Lallemand, L.-S. Luo, Multiple-relaxation-time lattice Boltzmann models in three dimensions, Phil. T. Roy. Soc. A 360 (1792) (2002) 437–451.
[9] U. Frisch, B. Hasslacher, Y. Pomeau, Lattice-Gas automata for the Navier–Stokes equation, Phys. Rev. Lett. 56 (14) (1986) 1505–1508.
[10] Z. Guo, T.S. Zhao, Lattice Boltzmann model for incompressible flows through porous media, Phys. Rev. E 66 (2002) 036304.
[11] J. Hardy, Y. Pomeau, O. de Pazzis, Time evolution of a two-dimensional model system. I. Invariant states and time correlation functions, J. Math. Phys. 14 (12) (1973) 1746–1759.
[12] P. Hariharan, M. Giarra, V. Reddy, S.W. Day, K.B. Manning, S. Deutsch, S.F.C. Stewart, M.R. Myers, M.R. Berman, G.W. Burgreen, E.G. Paterson, R.A. Malinauskas, Multilaboratory particle image velocimetry analysis of the FDA benchmark nozzle model to support validation of computational fluid dynamics simulations, J. Biomech. Eng. 133 (2011) 041002.
[13] S.E. Harrison, The use of the lattice Boltzmann method in thrombosis modelling, Ph.D. University of Sheffield, 2007.
[14] X. He, G. Duckwiler, D.J. Valentino, Lattice Boltzmann simulation of cerebral artery hemodynamics, Comput. Fluids 38 (4) (2009) 789–796.
[15] X. He, L-S. Luo, Lattice Boltzmann model for the incompressible Navier–Stokes equation, J. Stat. Phys. 88 (3/4) (1997) 927–944.
[16] X. He, L-S. Luo, Theory of the lattice Boltzmann method: From the Boltzmann equation to the lattice Boltzmann equation, Phys. Rev. E 56 (6) (1997) 6811–6817.
[17] F.J. Higuera, J. Jimnez, Boltzmann approach to lattice gas simulations, Europhys. Lett. 9 (7) (1989) 663–668.
[18] H. Huang, T.S. Lee, C. Shu, Lattice-BGK simulation of steady flow through vascular tubes with double constrictions, Int. J. Numer. Methods H 16 (2) (2006) 185–203.
[19] M. Junk, A. Klar, L-S. Luo, Asymptotic analysis of the lattice Boltzmann equation, J. Comput. Phys. 210 (2) (2005) 676–704.
[20] W.A. Kareem, S. Izawa, A.-K. Xiong, Y. Fukunishi, Lattice Boltzmann simulations of homogeneous isotropic turbulence, Comput. Math. Appl. 58 (5) (2009) 1055–1061.
[21] T. Krüger, F. Varnik, D. Raabe, Shear stress in lattice Boltzmann simulations, Phys. Rev. E 79 (2009) 046704.
[22] J. Latt, B. Chopard, Lattice Boltzmann method with regularized pre-collision distribution functions, Math. Comput. Simul. 72 (2-6) (2006) 165–168.
[23] G. Mayer, G. Házi, Direct numerical and large eddy simulation of longitudinal flow along triangular array of rods using the lattice Boltzmann method, Math. Comput. Simul. 72 (2-6) (2006) 173–178.
[24] G.R. McNamara, G. Zanetti, Use of the Boltzmann equation to simulate Lattice-Gas automata, Phys. Rev. Lett. 61 (20) (1988) 2332–2335.
[25] R. Mei, W. Shyy, D. Yu, L-S. Luo, Lattice Boltzmann method for 3-D flows with curved boundary, J. Comput. Phys. 161 (2) (2000) 680–699.
[26] O. Pelliccioni, M. Cerrolaza, M. Herrera, Lattice Boltzmann dynamic simulation of a mechanical heart valve device, Math. Comput. Simul. 75 (1-2) (2007) 1–14.
[27] Y.H. Qian, D. D'Humires, P. Lallemand, Lattice BGK models for Navier–Stokes equation, Europhys. Lett. 17 (6) (1992) 479–484.
[28] R. Rubinstein, L-S. Luo, Theory of the lattice Boltzmann equation: symmetry properties of discrete velocity sets, Phys. Rev. E 77 (2008) 036709.

[29] M. Tamagawa, H. Kaneda, M. Hiramoto, S. Nagahama, Simulation of thrombus formation in shear flows using lattice Boltzmann method, Artif. Organs 33 (8) (2009) 604–610.
[30] F. Toschi, S. Succi, Lattice Boltzmann method at finite Knudsen numbers, Europhys. Lett. 69 (4) (2005) 549–555.
[31] S. Wolfram, Cellular automaton fluids 1: Basic theory, J. Stat. Phys. 45 (3-4) (1986) 471–526.
[32] W.P. Yudistiawan, S.K. Kwak, D.V. Patil, S. Ansumali, Higher-order Galilean-invariant lattice Boltzmann model for microflows: single-component gas, Phys. Rev. E 82 (2010) 046701.
[33] R. Zhang, I. Staroselsky, H. Chen, Realization of isotropy of the lattice Boltzmann method via rotation of lattice velocity bases, J. Comput. Phys. 225 (2) (2007) 1262–1270.